J. Biophotonics **7**, No. 8, 647–655 (2014) / **DOI** 10.1002/jbio.201300081

Journal of BIOPHOTONICS

FULL ARTICLE

Effect of N-ethylmaleimide, chymotrypsin, and H_2O_2 on the viscoelasticity of human erythrocytes: Experimental measurement and theoretical analysis

Yin-Quan Chen[1], *Chih-Wei Chen*[1], *Yu-Li Ni*[2], *Yu-Shan Huang*[1], *Orson Lin*[3], *Shu Chien*[4], *Lanping Amy Sung*[*,4], *and Arthur Chiou*[*,1,5]

[1] Institute of Biophotonics, National Yang-Ming University, Taipei, Taiwan, ROC
[2] Department of Medicine, National Yang-Ming University, Taipei, Taiwan, ROC
[3] Department of Physics, National Tsing-Hua University, Hsinchu, Taiwan, ROC
[4] Department of Bioengineering and Institute of Engineering in Medicine, University of California, San Diego, California, USA
[5] Biophotonics & Molecular Imaging Research Center (BMIRC), National Yang-Ming University, Taipei, Taiwan, ROC

Received 22 May 2013, revised 25 July 2013, accepted 27 July 2013
Published online 22 August 2013

Key words: Viscoelaticity, Erythrocytes, Jumping optical tweezers, Kelvin's solid model, N-ethylmaleimide, Chymotrypsin, Hydrogen peroxide

Supporting information for this article is available free of charge under http://dx.doi.org/10.1002/jbio.201300081

The physiological functions of erythrocytes depend critically on their morphology, deformability, and aggregation capability in response to external physical and chemical stimuli. The dynamic deformability can be described in terms of their viscoelasticity. We applied jumping optical tweezers to trap and stretch individual red blood cells (RBCs) to characterize its viscoelasticity in terms of the Young's modulus and viscosity by analyzing the experimental data of dynamic deformation using a 2-parameter Kelvin solid model.

The effects of three chemical agents (*N*-ethylmaleimide, Chymotrypsin, and Hydrogen peroxide) on RBC's mechanical properties were studied by comparing the Young's modulus and viscosity of RBCs with and without these chemical treatments. Although the effects of each of these chemicals on the molecular structures of RBC may not be exclusive, based on the dominant effect of each chemical, we attempted to dissect the main contributions of different constituents of the RBC membrane to its viscosity and elasticity.

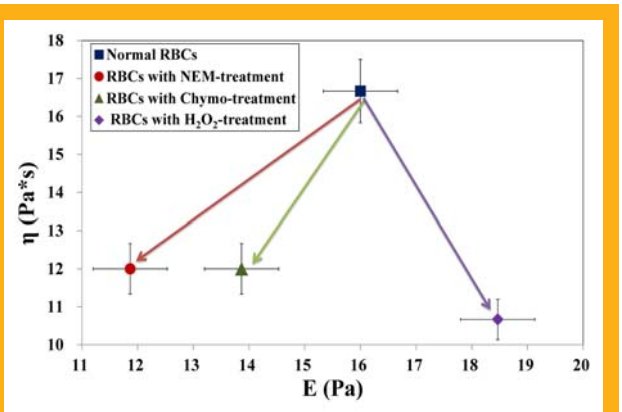

A summary of the effects of these three chemical agents on the mean values of E and η (obtained by averaging over 90 RBCs) is shown on a E-η plane. The lengths of the horizontal and the vertical bars around each point represent the corresponding SEMs of E and η, respectively.

* Corresponding authors: e-mail: amysung@ucsd.edu, Phone: +1-858-534-5250, Fax: +1-858-534-5722, aechiou@ym.edu.tw, Phone: +886-2-2823-7141, Fax: +886-2-2823-6314

Journal of BIOPHOTONICS

1. Introduction

The morphology and deformability of human red blood cells (RBCs) are critical for their physiological functions of oxygen transport and other tasks. Each RBC circulates through the entire body for almost 50,000 cycles, passing through capillaries with diameters as small as 3 microns during their 120-day lifespan. RBCs are able to withstand the shear stress during circulation owing to their unique viscoelasticity [1, 2]. Several methods have been developed to apply an external force to a biological cell either locally or distributed over the cell to probe its mechanical response [3–16]. These methods include optical magnetic twisting cytometry [3], optical tweezers with micro-beads (serving as handles) attached to RBCs [4, 12–14], optical tweezers dragging RBCs through viscous fluid [5], dual-trap optical tweezers [6], optical stretcher [7–9], micropipette aspiration [10, 11], RBC bending and relaxation via optical tweezers with triple-focal spots [15], and the RBC deformation and relaxation in a parallel-plate flow chamber [16]. Each of these methods has certain advantages and limitations, and often complements each other.

Several constituents of RBCs, such as the lipid membrane, the cytoskeleton, and the cytoplasm, contribute to the viscoelasticity of RBCs [11, 16, 17]. For example, membrane lipid bilayer contributes mainly to bending resistance [2], whereas the spectrin tetramers linked to the membrane protein band 3 by ankyrin and protein 4.2 play an important role in maintaining the elasticity of RBCs [18]. In pathological conditions, alterations of the biconcave-discoid morphology and the deformability of RBCs, due to insufficient or defective structural proteins [19], are believed to play important roles in diseases such as hereditary spherocytosis (HS) [20, 21], hereditary elliptocytosis (HE) [22], sickle cell disease (SCD) [23], and malaria-infected RBCs [24, 25]. Most of the previous biomechanical studies focused mainly on RBC elasticity, and much less on viscosity [12, 13].

In this study, we applied three chemical agents to induce different structural alterations in RBCs. Although the effects of each of these chemicals on the molecular structures of RBCs may be complicated and not exclusive, the following effects have been reported in the literatures: N-ethylmaleimide (NEM) dissociates spectrin tetramers into dimers [26, 27]; chymotrypsin (Chymo) cleaves ankyrin in RBC ghosts [26, 28] and digests extracellular domains of major transmembrane proteins band 3 and glycophorin A in intact RBCs [29]; and hydrogen peroxide (H_2O_2) causes lipid peroxidation and cross-linking of proteins including spectrin with hemoglobin and other membrane skeletal proteins as reported by Snyder et al. [31]. The effect of each agent on RBC viscoelasticity was quantified by measuring and comparing the Young's modulus (E) and the viscosity (η) of RBC samples with and without the chemical treatments. The measurements were accomplished by trapping and stretching individual human RBCs in a non-contact and non-invasive mode by using the jumping optical tweezers [30] and fitting the experimental data for the dynamic deformation of individual RBCs with a theoretical curve derived from the Kelvin solid model.

2. Experimental procedures

2.1 Preparation of human RBCs

A venous blood sample (3 mL) was obtained from a healthy volunteer by using the Becton Dickson (BD) Vacutainer (No. 36785) spray–coated with 5.4 mg K_2EDTA. After gentle inversion 8 to 10 times, 200 μl of blood sample from the Vacutainer was mixed with 200 μl of 0.9% saline in an Eppendorf tube and then centrifuged at 3,000 rpm at 4 °C for 10 minutes (Hsiangtai, Z233 MK-2, Taiwan) to separate the RBCs from the whole blood samples. The spun down RBCs were washed twice with 0.9% saline and collected from the bottom portion of the Eppendorf tube.

2.2 Preparation for N-ethylmaleimide (NEM) treatment

Previous results showed that 70% of spectrin tetramers were dissociated into dimers when RBC ghosts were treated with N-ethylmaleimide (NEM) [26]. For the treatment of RBC samples with NEM, we followed the procedure and the concentration suggested by Sleep et al. [26]; briefly, 2 mM of NEM (Sigma-Aldrich E3876) in 0.9% saline (1 ml) was added to the prepared RBCs (10 μl, containing ~10^8 cells) and shaken gently at room temperature for 1 hour. The NEM-treated RBCs were centrifuged (at 3,000 rpm at 4 °C for 10 minutes) and the supernatant was removed. The NEM-treated RBCs were then washed three more times with 0.9% saline.

2.3 Preparation for Chymotrypsin (Chymo) treatment

For the treatment of RBCs with Chymo, we followed the procedure and the concentration suggested by Sleep et al. [26], who reported that all ankyrin in

RBC ghosts was cleavage in 10 mg/ml of Chymo solution. Briefly, 10 mg/ml of Chymo (Sigma-Aldrich C3142) in 0.9% saline (1 ml) was mixed with 10 µl of prepared RBCs (containing ~10^8 cells) and shaken gently at room temperature for 1 hour. The Chymo-treated RBCs were centrifuged (at 3,000 rpm at 4 °C for 10 minutes) and the supernatant was removed. The Chymo-treated RBCs were then washed three more times with 0.9% saline.

2.4 Preparation for hydrogen peroxide (H_2O_2) treatment

For the treatment of RBCs with H_2O_2, the procedure and the concentration suggested by Snyder et al. [31] were adopted; briefly, 100 µM of H_2O_2 (Sigma-Aldrich) in 0.9% saline (1 ml) was mixed with 10 µl of prepared RBCs (containing ~10^8 cells) and shaken gently at room temperature for 15 minutes. The H_2O_2-treated RBCs were centrifuged (at 3,000 rpm at 4 °C for 10 minutes) and the supernatant was removed. The H_2O_2-treated RBCs were then washed with 0.9% saline three more times.

2.5 RBC samples selection

To avoid the variations in experimental data caused by the differences in size and morphology from one RBC sample to another, we made all measurements on samples (including those subjected to chemical treatment) with RBC diameter in the range of 7.2 to 7.6 µm in the relaxed phase and maintaining a biconcave morphology. Any RBC samples severely affected by the chemical treatment to exhibit visible morphological damage were excluded in our measurements. Hence, the effects of chemical treatments reported in this paper could be systematically under-estimated, because those samples with severe alterations in size or morphology by chemical treatment were excluded in our measurements. On average, the percentages of RBCs excluded from our measurements upon visual inspection under a microscope were 10%, 11%, and 14%, for chemical treatments with NEM, Chymo, and H_2O_2, respectively.

2.6 Jumping optical tweezers

Our jumping optical tweezers system is shown in Figure 1 [30]. A $Nd:YVO_4$ laser beam ($\lambda = 1064$ nm) serving as the trapping beam was collimated and expanded to a beam diameter of 3 mm via a pair of convex lenses ($f_1 = 10$ cm, $f_2 = 20$ cm) in a telescopic arrangement, and passed through an acousto-optic modulator (AOM; intraAction corp & DTD-274HD6M) at Bragg angle; the zero order transmitted beam was blocked and the 1st order diffracted beam was directed towards a pair of relay lens ($f_3 = 12$ cm, $f_4 = 24$ cm) in a telescopic arrangement, which imaged the exit aperture of the AOM onto the entrance aperture of an oil-immersed microscope objective lens (100X, $NA = 1.3$) such that the angular scan of the beam by the AOM was transformed into a lateral displacement of the focal spot of the laser beam at the focal plane of the microscope objective without any beam walk-off at the entrance aperture of the objective. The diffraction an-

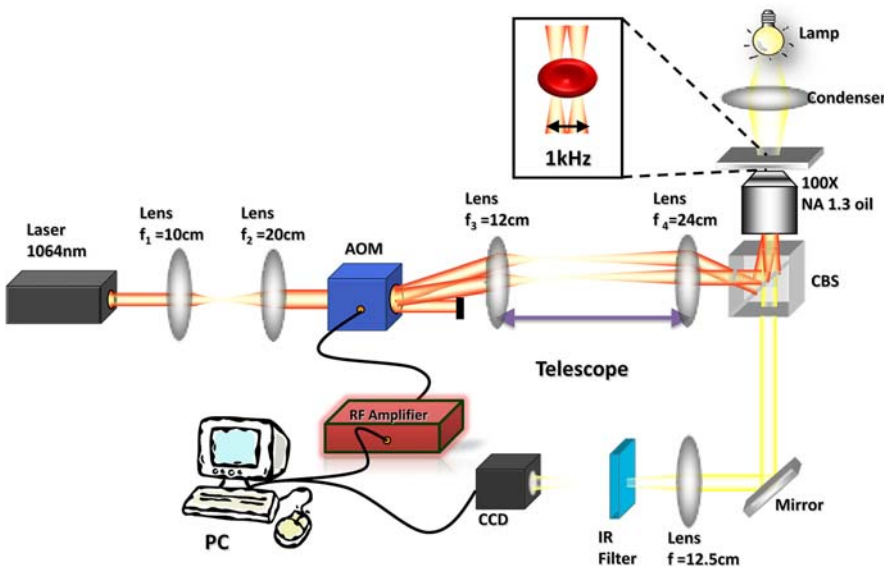

Figure 1 A schematic diagram of the jumping optical tweezers setup.

gle of the output beam was controlled by applying appropriate radio-frequency (RF, 30 to 50 MHz) signals to the AOM. The focal spot of the trapping beam was scanned discretely between two fixed points (referred to as the jumping distance) by switching the driving radio-frequency between two fixed values. We have shown that such a system can trap and stretch individual human RBCs efficiently without any mechanical contact and with no detectable optical damage (for trapping and stretching optical power on the order of 12 mW at $\lambda = 1064$ nm) [30]. A white light source (Taiwan fiber optics, LSH150F) was used to illuminate the trapped RBC sample for imaging via a charged-coupled device (CCD, WAT-120N) linked to a computer for digital recording and processing. An infrared (IR) filter in front of the CCD camera served to block the IR trapping beam (reflected and back-scattered by the sample and by other optical interfaces and elements) from entering into the CCD camera.

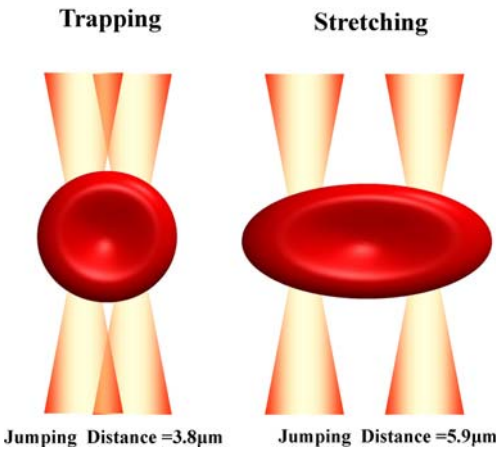

Figure 2 A schematic diagram illustrating how a RBC was trapped (at a jumping distance of 3.8 μm) and stretched (at a jumping distance of 5.9 μm) by jumping optical tweezers. The jumping distance is defined as the distance between the two focal spots of the jumping (or discretely scanned) laser beam.

2.7 Dynamic deformation of red blood cells

The trapping laser beam spot ($\lambda = 1064$ nm; trapping power ~12 mW) in a jumping optical tweezers system [30] was discretely scanned between two fixed points via an acousto-optic modulator (AOM) with a scanning frequency of 1 KHz. At this scanning frequency, the two focal points can be regarded as a pair of parallel tweezers capable of trapping and stretching individual RBCs. For jumping distance (defined as the distance between the two jumping laser beam spots) in the range of approximately 3 to 6 μm, the stretching force on the trapped RBC sample increases as the jumping distance increases [30]. By switching the jumping distance back and forth periodically between a smaller distance of 3.8 μm and a larger distance of 5.9 μm, the trapped RBC was periodically stretched and relaxed (Figure 2). The dynamic deformation of RBCs between alternating phases of stretching and recovery was recorded (Figure 3).

2.8 Theoretical fits to experimental data and analysis

We applied the classical Kelvin solid model, as shown in the upper left corner in Figure 4(a), to fit our experimental data to characterize the viscoelasticity of each RBC in terms of its Young's modulus and viscosity. The differential equation of the system can be expressed as [33]

$$\sigma(t) = E\varepsilon(t) + \eta\dot{\varepsilon}(t) \tag{1}$$

where $\sigma(t)$ is the stress (as a function of time); and $\varepsilon(t)$ is strain (as a function of time); "E" is the Young's modulus of the elastic element, "η" the viscosity of the viscous element, and the "dot" represents the time-derivative.

The solution of the differential Eq. (1) is

$$\varepsilon(t) = \frac{\sigma_0}{E}[1 - \mathrm{e}^{-(E/\eta)t}] = a[1 - \mathrm{e}^{-bt}] \tag{2}$$

When the jumping distance of the optical tweezers was abruptly switched from 3.8 μm to 5.9 μm at time

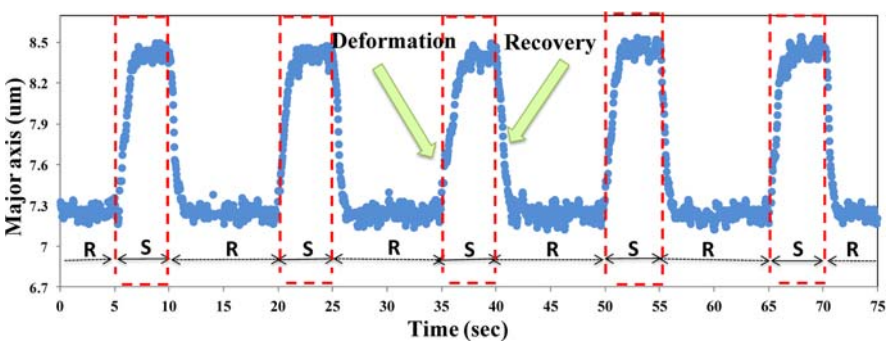

Figure 3 Typical experimental results representing the dynamic deformation of RBCs in response to a periodic stretch-and-relax force (in the form of a periodic step function) derived from the jumping optical tweezers; each period consists of a 5-sec stretch phase "S" and a 10-sec relax phase "R".

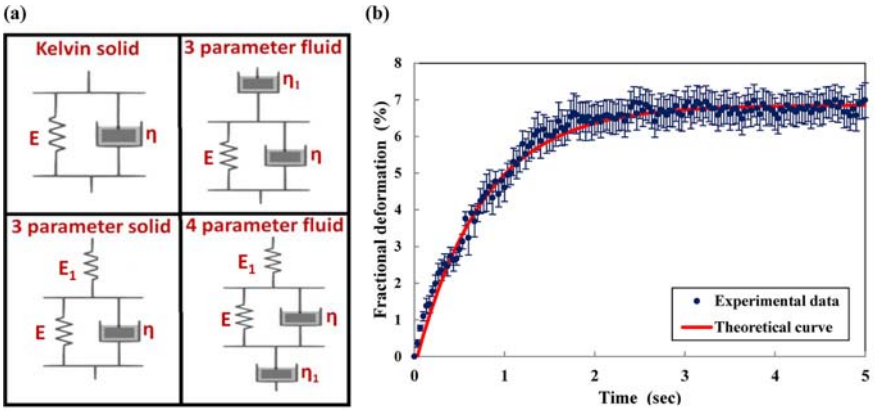

Figure 4 (a) Four classical mechanical models for the characterization of a viscoelastic material or system in terms of one or more Young's modulus and viscosity; (**b**) Experimental data showing the fractional deformation of an optically trapped human RBC as a function of time when stretched by optical force in jumping optical tweezers for 5 sec in the form of a step function. The experimental data represent the mean value obtained by averaging over an individual RBC with three repeated measurements; the associated standard error of the mean (SEM) is represented by the thin vertical line. The solid line represents the theoretical fit based on the Kelvin solid model [Eq. (2)].

$t = 0$ sec, we assumed that the stress σ_0 on the RBC sample changed approximately from 0 to 1.0 N/m^2 [34] (laser power = 6 mW per trap at the trapping zone) in the form of a step function. The resulting fractional deformation (or strain) $\varepsilon(t) = [r(t) - r_0]/r_0$, where r_0 is the major axis length of RBCs in the relax state (i.e., at the smaller jumping distance of 3.8 μm), and $r(t)$ is the major axis length as a function of time in the stretched state (i.e., when the jumping distance was switched from 3.8 μm to 5.9 μm at time $t = 0$ sec, and maintained at 5.9 μm from $t = 0$ sec to $t = 5$ sec). The experimental data (representing the mean value obtained by averaging the measured results from an individual RBC with three repeated measurements) were fitted with Eq. (2) using two fitting parameters ($a = \sigma_0/E$ and $b = E/\eta$), as shown in Figure 4(b).

In addition to the theoretical fit to the Kelvin's solid model to characterize the viscoelasticity of each RBC in terms of (E) and (η) as discussed in the previous sections, we also applied the 3-parameter fluid model, the 3-parameter solid model, and the 4-parameter fluid model [Figure 4(a)] to fit our experimental data. The results (not shown) indicate that the additional serial viscous elements, with viscosity η_1 in the 3-parameter fluid and the 4-parameter fluid models [the right hand side of Figure 4(a)], and the additional elastic elements, with Young's modulus E_1 in the 3-parameter solid and the 4-parameter fluid models [the lower part of Figure 4(a)], do not provide any additional information because the contributions of both η_1 and E_1 to the viscoelasticity of the system are negligible. In summary, of the four classical models shown in Figure 4(a), the Kelvin solid model represents a simple and yet useful model compatible with our experimental approach to characterize the viscoelasticity of RBCs in terms of a single elastic element and a single viscous element in parallel, despite the fact that the model is a marked simplification and does not resemble at all the physical morphology and structure of a biconcave RBC.

3. Experimental results and discussion

The fractional deformations of RBCs (with and without chemical treatment) as a function of time in response to a step optical stretch were recorded and compared in Figure 5. We fitted the experimental data of the dynamic fractional deformation of each individual RBC (averaging over three repeated measurements) to the Kelvin solid model to obtain E and η for each RBC, the mean values and the standard error of the mean (SEM) of E and η obtained from 90 RBCs are shown in Figure 6(a) and (b), respectively.

The Kelvin solid model, represented by Eq. (2) above, characterizes a complex system or material (in this specific case, individual RBCs) with one discrete elastic element (with Young's modulus E) and one discrete viscous element (with viscosity η) in parallel, when the time-dependent strain $\varepsilon(t)$ in response to a stress σ_0 (in the form of a step function at $t = 0$) fits an exponential function $\varepsilon(t) = a[1 - e^{-bt}]$ with a single time constant $\tau = 1/b$. In curve fitting of this equation to our experimental data with two fitting parameters "a" and "b", the relationship between the physical parameters (E, η, and σ_0) and the geometrical parameters (a and b) of the exponential curves can be summarized as follow:

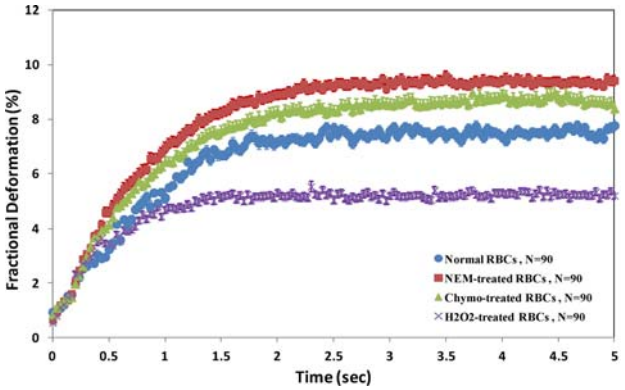

Figure 5 A comparison of the dynamic fractional deformation of RBCs without (in blue) and with chemical treatments of NEM (in red), Chymo (in green), and H_2O_2 (in purple). The mean values, obtained by averaging over 90 RBCs, are indicated by the solid symbols and the associated standard error of the mean (SEM) by the thin vertical lines. The concentration of each chemical and the detail procedures are described in the "Method" Section.

the time constant $\tau = 1/b = \eta/E$;

the steady-state strain $\varepsilon_{SS} = \varepsilon(t)|_{t\to\infty} = a = \sigma_0/E$;

the initial slope $\dot{\varepsilon}(0) = \dot{\varepsilon}(t)|_{t\to 0} = ab = \sigma_0/\eta$.

These expressions can be rewritten as

$E = \sigma_0/\varepsilon_{SS}$;

$\eta = \sigma_0/\dot{\varepsilon}(0)$;

$E/\eta = 1/\tau$.

Hence, both the absolute values of E and η scale with the stress σ_0, which needs to be determined independently. In this analysis the membrane thickness is not needed.

However, in many other physical models reported in the Refs. [13, 17, 35–37], the mechanical and viscoelastic properties of RBCs are characterized by the shear modulus μ_0, viscosity (of the membrane, the cytosol, and the external fluid), and bending resistance (or rigidity). Apparently, the bending resistance does not appear in the Kelvin solid model; the shear modulus, however, can be estimated by the approximation $\mu_0 = Eh$, where "h" is the thickness of the membrane. Under this assumption, $\mu_0 = hE = h\sigma_0/\varepsilon_{SS}$, scales linearly with the product of the membrane thickness "h" and the constant stress σ_0.

Even though the thickness of the lipid bilayer is only a few nm, the effective thickness of the cell membrane, h, including the membrane skeleton and the extracellular carbohydrate moiety, may be tens or hundreds of nm [38, 39]. Thus in digital simulations of RBCs' mechanics reported in the Refs. [34, 40–42], various values of h within the range of several tens to several hundreds nm have been assumed as a

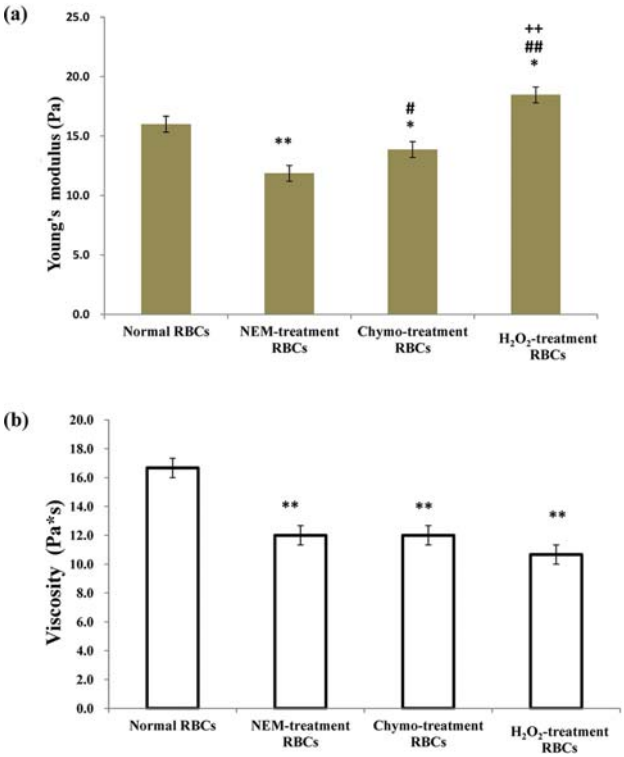

Figure 6 The mean values (obtained by averaging over 90 individual RBCs) of (**a**) the Young's modulus (E) and (**b**) the viscosity (η) of RBCs, with and without chemical treatments of NEM, Chymo, and H_2O_2. The mean values are indicated by the height of the thick bars and the associated SEM by the thin vertical lines. Statistical significance of the experimental results was evaluated by a one-way variance analysis (ANOVA) with LSD post-hoc test. Significant differences from "Normal RBCs" are designated by * $P < 0.05$ and ** $P < 0.001$. In (**a**), significant differences from "NEM-treated RBCs" are indicated by # $P < 0.05$ and ## $P < 0.001$, and from "Chymo-treated RBCs" by ++ $P < 0.001$. In (**b**) the differences in the results among the three types of chemical treatments are statistically insignificant.

compromise to the computation time and complexity. For examples, in our recent modeling of 3-dimensional deformation of individual biconcave RBCs trapped and stretched by a pair of identical parallel optical traps (without any beads attached to the RBCs) by either photon momentum transfer based on Ray-Optics Model [34], or by Maxwell tensor based on EM Model [42], we have assumed the effective membrane thickness to be ~ a few hundreds nm, and the maximum constant stress is estimated to be on the order of 1 Pa, when the distance between the two trapping foci is about 6 μm. Note that the stress distribution (on RBC) obtained by this approach is much more uniform compared with the approach reported in the Refs. [4, 12, 13], where two beads were attached diagonally across the diameter

of the RBC and with RBC stretched by two optical traps, one on each bead (which serves as the handle). Besides, the net maximum stress causing the BRC elongation is also expected to be much weaker when the RBC is trapped and stretched by dual parallel optical tweezers without beads as handles.

In this study, if we assume the constant stress $\sigma_0 = 1$ Pa, and the effective membrane thickness $h = 10$ nm, then for normal RBCs without chemical treatment, we would obtain the following results:

Young's modulus $E = \sigma_0/\varepsilon_{SS} = (16.0 \pm 0.7)$ Pa;

viscosity $\eta = \sigma_0/\varepsilon'(0) = (16.7 \pm 0.7)$ Pa · s;

the ratio $E/\eta = \tau = 0.9 \pm 0.1$ s;

shear modulus $\mu_0 = h/\sigma_0\varepsilon_{SS} = 0.16$ pN/μm.

These values are consistent with those reported in the Refs. [4, 12, 36], despite the fact that in the Kelvin solid model, the Young's modulus E and the viscosity η represent, at the best, a macroscopic overall viscoelasticity of RBCs. Admittedly such simplified model does not allow us to dissect the contributions from individual constituents (such as lipid bilayer, spectrin network, anchoring proteins, and cytosol) unless the effect of different chemical treatments with high-specificity (i.e., each chemical influences only one specific individual constituent) can be tested.

Figure 5 compares the dynamic fractional deformation of normal RBCs with those under chemical treatments, from which the values of the Young's modulus E and the viscosity η were deduced for each case; the corresponding results are compared in Figure 6.

After NEM treatment, E dropped by 26% (from 16.0 ± 0.7 to 11.9 ± 0.7 Pa; $p < 0.001$), and η dropped by 28% (from 16.7 ± 0.7 to 12.0 ± 0.7 Pa · s; $p < 0.001$), implying respectively that the RBCs became "less elastic" and "more fluidic" after the dissociation of spectrin tetramers into dimers by NEM. Figure 7 illustrates the normal erythrocyte membrane, consisting of the lipid bilayer and the membrane skeletal network, including the transmembrane proteins [43]. Thus the NEM treatment may lessen the number of the head-to-head association of $\lambda\beta$ sprectin dimers in the network, leading to the alteration of the topology of the membrane skeleton.

In the case of Chymo treatment, E decreased by 13% (from 16.0 ± 0.7 to 13.9 ± 0.7 Pa; $p < 0.05$) and η decreased by 28% (from 16.7 ± 0.7 to 12.0 ± 0.7 Pa · s; $p < 0.001$), implying that a normal linkage of the spectrin skeleton to the lipid bilayer of the cell membrane through intact suspension complexes may be necessary for RBCs to maintain their elasticity and viscosity. Since Chymo treatment may digest the extracellular domains of band 3 and glycophorin A at the suspension complex, as well as glycophorin C

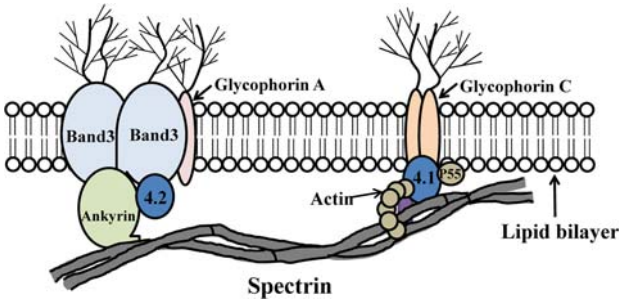

Figure 7 The side view of the erythrocyte membrane, showing the lipid bilayer and membrane skeletal network. The carbohydrate moieties of the major transmembrane band 3, glycophorins on the cell surface are also shown. Left complex: Suspension complex; right complex: junctional complex (adapted from Ref. [43]). For the detailed spectrin-actin-protein 4.1 tertiary complex in a wrap-around model, please see Sung and Vera, 2003 and Sche, Vera, and Sung, 2011.

associated with the junctional complex, such treatment may remove not only portions of the extracellular domain of these major transmembrane proteins, but also the significant carbohydrate moieties of these glycoproteins. The former may lead to the instability or disintegration of the suspension complex, and the latter the reduction of resistance for suspension and junctional complexes if they need to move through the lipid bilayer during deformation.

Treatment with H_2O_2 caused E to increase by 15% (from 16.0 ± 0.7 to 18.5 ± 0.7 Pa; $p < 0.05$) and η to decrease by 36% (from 16.7 ± 0.7 to 10.7 ± 0.7 Pa · s; $p < 0.001$). These results indicated that such treatment known to induce peroxidation of the lipid and cross-linking of erythrocyte proteins reduced the viscosity more so than reducing the elastic modulus. Even though peroxidation of the lipd bilayer did not alter the deformability of RBCs [31], results here did not exclude the possibility that lipid peroxidation may participate in the alternation of η. Since H_2O_2 treatment induced cross-linking of spectrin, especially λ spectrin, with hemoglobin and other membrane skeletal proteins [31], potentially including that in the spectrin-actin-protein 4.1 tertiary complex [32], the normal redox state of the lipid bilayer and the membrane skeletal proteins contribute to both viscosity and elasticity of RBCs under physiological condition.

As noted earlier, since the effects of each of these chemicals on the molecular structures are by no means specific or exclusive, detailed biochemical analyses (which is beyond the scope of this paper) will be required to further dissect the effects of each chemical [44, 45] to tell a more complete story.

The key experimental results discussed above are summarized graphically in the form of a 2-dimensional (E, η) plot in Figure 8.

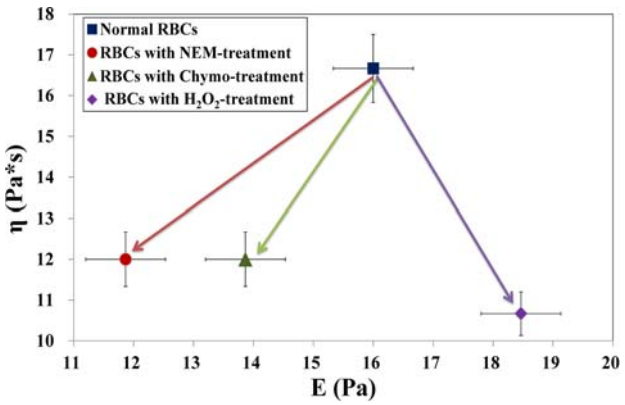

Figure 8 A summary of the effects of the three different kinds of chemical agents (namely NEM, Chymo, and H_2O_2) on the mean values of E and η (obtained by averaging over 90 RBCs) is shown on a E-η plane. The lengths of the horizontal and the vertical bars around each point represent the corresponding SEMs of E and η, respectively.

4. Summary and conclusions

Although the viscoelasticity of RBCs has been studied extensively, our approach has several important features that distinguish it from the previous works and provides some new insights. Most of the earlier studies [26, 46–48] focused more on the RBC elasticity than viscosity; only a few studies of RBC viscosity have been reported recently [13, 35, 36, 49, 50]. Many earlier works have implied that lipids are the main contributor to viscosity and that the cytoskeleton is mainly responsible for elasticity (e.g., Fedosov et al. [51]). However, our results (Figure 6) imply that (a) the spectrin may play a nearly equal role in RBC elasticity and viscosity, and that (b) the anchoring of RBC lipid membrane to spectrin network by band 3 and glycophorins may contribute to RBC viscosity more than elasticity.

Of the three chemical agents tested in our study, H_2O_2 is the only one that resulted in different trend of changes of RBC as it raised elastic modulus by +15% and reduced the viscosity to a greater degree by −36%. One major effect of H_2O_2 is often interpreted as cellular damage due to oxidative stress including cross-linking membrane and cytosolic proteins. An increase in human RBC rigidity has been reported by Machiedo et al. [46] on patients with sepsis, by Cicha et al. [47] on the effect of oxidative injury caused by either diamide (azo-dicarboxylic acid-bis-*N,N*-dimethyl-amide) or Fe^{2+}/ascorbate, and also by Snyder et al. [31] on H_2O_2 treatment. It is reasonable to expect that when cell membrane proteins are cross-linked, the elastic modulus would increase.

In summary, we have demonstrated that when a human RBC, in its intact biconcave morphology, was stretched by an optical stretching force approximated by a step function (generated via jumping optical tweezers), the fractional deformation as a function of time followed a simple exponential function which can be fitted to the Kelvin solid model to deduce its elasticity and viscosity. Using this approach, we have measured the elasticity and viscosity of RBC samples with and without three different chemical treatments to probe the possible roles of spectrin, band 3 and glycophorins, and the effect of oxidative stress on RBCs' viscoelasticity. Even though the effects of each of these chemicals on the molecular structures of RBC may not be absolutely exclusive (i.e., may be more extensive or complicated), but if we consider only the major effects reported in the literatures, our results (based on the percentage change of elasticity and viscosity before and after each treatment; see Figure 8) suggest that (a) the horizontal connectivity or the topology of the spectrin network contributes approximately equally to RBC elasticity and viscosity; (b) the vertical anchoring of RBC membrane to spectrin network (through band 3 and glycophorin A at the suspension complex and glycophorin C at the junctional complex) is critical in maintaining the RBC viscosity much more than its elasticity; (c) the oxidative stress induced by H_2O_2, led to opposite effects on RBC elasticity and viscosity, and the resulting fractional reduction in viscosity is more than three times the fractional increment in elastic modulus; and (d) the dissociation of spectrin from tetramer to dimer by NEM and the chymotrypsin digestion of band 3 and glycophorins appear to reduce RBC viscosity by the same degree, but slightly less than the corresponding reduction caused by H_2O_2.

Acknowledgements This work is jointly supported by The National Science Council, Taiwan, ROC (Projects No. NSC98–2627-M010–004 & NSC99–2923-E-010–001-MY3; I-RiCE Program, Project No. NSC-99–2911-I-010–101 & NSC-100–2911-009–101) and by the Ministry of Education (The Top University Project).

Author biographies Please see Supporting Information online.

References

[1] Y. Fung, Biomechanics: mechanical properties of living tissues (Springer-Verlag, New York, 1993), pp. 101–130.
[2] M. Diez-Silva, M. Dao, J. Han, C. T. Lim, and S. Suresh, MRS Bull. **35**, 382–388 (2010).
[3] M. Puig-de-Morales-Marinkovic, K. T. Turner, J. P. Butler, J. J. Fredberg, and S. Suresh, Am. J. Physiol.-Cell Physiol. **293**, 597–605 (2007).

[4] S. Henon, G. Lenormand, A. Richert, and F. Gallet, Biophys. J. **76**, 1145–1151 (1999).
[5] M. Brandao, A. Fontes, M. Barjas-Castro, L. Barbosa, F. Costa, C. Cesar, and S. Saad, Eur. J. Haematol. **70**, 207–211 (2003).
[6] S. Rancourt-Grenier, M. T. Wei, J. J. Bai, A. Chiou, P. P. Bareil, P. L. Duval, and Y. Sheng, Opt. Express **18**, 10462–10472 (2010).
[7] J. Guck, R. Ananthakrishnan, H. Mahmood, T. J. Moon, C. C. Cunningham, and J. Käs, Biophys. J. **81**, 767–784 (2001).
[8] P. B. Bareil, Y. Sheng, Y. Q. Chen, and A. Chiou, Opt. Express **15**, 16029–16034 (2007).
[9] P. B. Bareil, Y. Sheng, and A. Chiou, Opt. Express **14**, 12503–12509 (2006).
[10] E. Evans, Biophys. J. **13**, 941–954 (1973).
[11] S. Chien, Rev. Physiol. **49**, 177–192 (1987).
[12] J. Mills, L. Qie, M. Dao, C. Lim, and S. Suresh, Mol. Cell. Biomech. **1**, 169–180 (2004).
[13] Y. Z. Yoon, J. Kotar, A. T. Brown, and P. Cicuta, Soft Matter **7**, 2042–2051 (2011).
[14] M. Dao, C. Lim, and S. Suresh, J. Mech. Phys. Solids **51**, 2259–2280 (2003).
[15] P. Bronkhorst, G. Streekstra, J. Grimbergen, E. Nijhof, J. Sixma, and G. Brakenhoff, Biophys. J. **69**, 1666–1673 (1995).
[16] S. Noji, S. Taniguchi, and H. Kon, Biophys. J. **52**, 221–227 (1987).
[17] D. A. Fedosov, B. Caswell, and G. E. Karniadakis, Biophys. J. **98**, 2215–2225 (2010).
[18] A. J. Bruce Alberts, Julian Lewis, Martin Raff, Keith Roberts, and Peter Walter, Molecular Biology of the Cell, (Garland Science, New York, 2002).
[19] P. G. Gallagher, Hematology **2005**, 13–18 (2005).
[20] P. Agre, E. P. Orringer, and V. Bennett, N. Engl. J. Med. **306**, 1155–1161 (1982).
[21] G. Tchernia, N. Mohandas, and S. Shohet, J. Clin. Invest. **68**, 454–460 (1981).
[22] S. Suresh, J. Mater. Res **21**, 1871–1877 (2006).
[23] S. H. Embury, R. Hebbel, N. Mohandas, and M. Steinberg, Sickle cell disease: basic principles and clinical practice, (Lippincott Williams & Wilkins, 1994), pp. 205–217.
[24] F. K. Glenister, R. L. Coppel, A. F. Cowman, N. Mohandas, and B. M. Cooke, Blood, **99**, 1060–1063 (2002).
[25] R. Suwanarusk, B. M. Cooke, A. M. Dondorp, K. Silamut, J. Sattabongkot, N. J. White, and R. Udomsangpetch, J. Infect. Dis. **189**, 190–194 (2004).
[26] J. Sleep, D. Wilson, R. Simmons, and W. Gratzer, Biophys. J. **77**, 3085–3095 (1999).
[27] T. Fischer, C. Haest, M. Stöhr, D. Kamp, and B. Deuticke, BBA. Biomembranes. **510**, 270–282 (1978).
[28] J. C. Pinder, A. Pekrun, A. Maggs, A. Brain, and W. Gratzer, Blood **85**, 2951–2961 (1995).
[29] L. J. Bruce, J. D. Groves, Y. Okubo, B. Thilaganathan, and M. Tanner, Blood **84**, 916–922 (1994).
[30] G. B. Liao, P. B. Bareil, Y. Sheng, and A. Chiou, Opt. Express **16**, 1996–2004 (2008).
[31] L. Snyder, N. Fortier, J. Trainor, J. Jacobs, L. Leb, B. Lubin, D. Chiu, S. Shohet, and N. Mohandas, J. Clin. Invest. **76**, 1971–1977 (1985).
[32] L. C. Wolfe, A. M. Byrne, and S. E. Lux, J. Clin. Invest. **78**, 1681–1686 (1986).
[33] W. Flugge, Viscoelasticity, (Springer-Verlag, New York, 1975), pp. 7–17.
[34] G. B. Liao, Y. Q. Chen, P. B. Bareil, Y. Sheng, A. Chiou, and M. S. Chang, (submitted to J. Biophotonics).
[35] R. Wang, H. Ding, M. Mir, K. Tangella, and G. Popescu, Biomed. Opt. Express **2**, 485–490 (2011).
[36] T. Betz, M. Lenz, J.-F. Joanny, and C. Sykes, PNAS **106**, 15320–15325 (2009).
[37] Y.-Z. Yoon, H. Hong, A. Brown, D. C. Kim, D. J. Kang, V. L. Lew, and P. Cicuta, Biophys. J. **97**, 1606–1615 (2009).
[38] H. Curtis and Sue N. Barnes., Biology. 5th ed. (World Publishers, New York, 1989). pp. 104.
[39] R. Hine, The Facts on File Dictionary of Biology (Checkmark, New York, 1999). pp. 198.
[40] V. Heinrich, K. Ritchie, N. Mohandas, and E. Evans, Biophys. J. **81**, 1452–1463 (2001).
[41] L. Boudin, C. Grandmont, Y. Maday, B. Maury, B. Sapoval, and J. F. Gerbeau, ESAIM: Proceedings **23**, 48–65 (2008).
[42] L. Yu, Y. Sheng, and A. Chiou, Opt. Express **21**, 12174–12184 (2013).
[43] P. G. Gallagher, Red cell membrane disorders, ASH Education Program Book, **2005**, 13–18 (2005).
[44] P. Hilarius, I. Ebbing, D. Dekkers, J. Lagerberg, D. De Korte, and A. Verhoeven, Biochemistry **43**, 4012–4019 (2004).
[45] L. Romano, A. Sidoti, G. De Luca, T. Gugliotta, P. Romano, A. Scuteri, and A. Amato, Cell Biochem. Funct. **20**, 99–102 (2002).
[46] G. W. Machiedo, R. J. Powell, B. F. Rush Jr, N. I. Swislocki, and G. Dikdan, Arch. Surg. **124**, 1386–1389 (1989).
[47] I. Cicha, Y. Suzuki, N. Tateishi, and N. Maeda, Pathophysiology **6**, 103–110 (1999).
[48] O. K. Baskurt, D. Gelmont, and H. J. Meiselman, Am. J. Respir. Crit. Care Med. **157**, 421–427 (1998).
[49] Y. Z. Yoon, H. Hong, A. Brown, D. C. Kim, D. J. Kang, V. L. Lew, and P. Cicuta, Biophys. J. **97**, 1606–1615 (2009).
[50] T. Betz, M. Lenz, J. F. Joanny, and C. Sykes, PNAS **106**, 15320–15325 (2009).
[51] D. A. Fedosov, B. Caswell, and G. E. Karniadakis, Biophys. J. **98**, 2215–2225 (2010).